Guidelines for the Voltammetric Study of Electrode Reactions with Coupled Chemical Kinetics at an Arbitrary Electrode Geometry

Manuela López-Tenés[a], Eduardo Laborda[a], Angela Molina*[,a], Richard G. Compton[b]

[a] *Departamento de Química Física, Facultad de Química, Regional Campus of International Excellence "Campus Mare Nostrum", Universidad de Murcia, 30100 Murcia, Spain*

[b] *Department of Chemistry, Physical & Theoretical Chemistry Laboratory, Oxford University, South Parks Road, OX1 3QZ Oxford, United Kingdom*

* Corresponding author:

Tel: +34 868 88 7524

Fax: +34 868 88 4148

Email: amolina@um.es

ABSTRACT

A powerful, unified and simplifying mathematical approach for the theoretical treatment of first-order chemical kinetics coupled to interfacial charge transfers at electrode of arbitrary geometry and size, both uniformly accessible and non-uniformly accessible to the electroactive species, is presented. The general CEC mechanism at spherical and disc electrodes is considered to test the validity and benefits of such approach, based on the application of the so-called kinetic steady state, that enables the reduction of the multivariable problem of kinetic-diffusive differential equations to a single variable problem of a diffusion-only differential equation. This is solved both analytically and numerically, showing how this approach leads to general, simple and efficient solutions for the study of the influence of coupled chemical kinetics on the voltammetric response.

The voltammetry of the CEC mechanism is analyzed as a function of the kinetics and thermodynamics of the preceding and subsequent chemical reactions and of the electrode size (from macroelectrodes to ultramicroelectrodes) and shape (spherical and disc). Comparison with the responses of the CE, EC and E mechanisms is included, proposing diagnosis criteria and procedures for quantitative analysis of experimental data.

INTRODUCTION

The electroactive species involved in charge transfer (CT) processes very usually undergo chemical reactions in solution such as complexations, protonations, isomerizations, re-arrangements, dimerizations, etc.[1–5]. The CEC mechanism (Scheme (I)), found for example in the electrochemistry of α-dicarbonyl compounds[6], thiols[7] and catechols/quinones[8,9], enables us to look into very different situations depending on whether both (CEC scheme), one (CE and EC schemes) or none (E mechanism) of the electroactive species undergo homogeneous chemical transformations:

$$B \underset{k_2}{\overset{k_1}{\rightleftarrows}} C \; ; \quad C + e^- \rightleftarrows D; \quad D \underset{k_4}{\overset{k_3}{\rightleftarrows}} E \tag{I}$$

with k_1 and k_2 as the forward and backward rate constants, respectively, of the chemical reaction preceding the CT, and k_3 and k_4 as the forward and backward rate constants of the reaction subsequent to the CT. Thus, we can introduce the following definitions:

$$K_1 = \frac{k_2}{k_1} = \frac{c_B^*}{c_C^*} \quad , \quad K_2 = \frac{k_3}{k_4} = \frac{c_E^*}{c_D^*} \tag{1}$$

$$\kappa_1 = k_1 + k_2 \quad , \quad \kappa_2 = k_3 + k_4 \tag{2}$$

where c_i^* is the equilibrium concentration of species *i* (≡ B, C, D, E). The CE and EC mechanisms are particular cases where $K_2 \to 0$ and $K_1 \to 0$, respectively, as well as the E mechanism where both conditions ($K_1 \to 0$ and $K_2 \to 0$) apply simultaneously.

Regarding the theoretical modelling of reaction mechanisms in interfacial electrochemistry, the problem initially implies the resolution of as many differential equations as chemical species involved in the reaction mechanism. In general, this makes the mathematical resolution more difficult, demanding and time-consuming than for the simple E mechanism. Nevertheless, by applying the kinetic steady state (kss) treatment[10–12], we have recently demonstrated that, under linear diffusion conditions, the problem of the Nernstian CEC mechanism given in Scheme (I) can be reduced from four to a single variable problem that is formally-identical to that of the non-Nernstian E mechanism (E_{irrev})[13]. This simplifies and

accelerates significantly the resolution of the problem and the resulting general solution covers a wide variety of electrochemical systems.

Given the value of microelectrodes (study of very fast kinetics, measurements in resistive media, reduced capacitive currents, miniaturization and simplification of instrumentation, high spatial resolution, …)[1,2,4,14], in this work the generalized and simplified treatment above-mentioned is extended and proven for other diffusion field geometries, including uniformly-accessible (as (hemi)spherical) and non-uniformly accessible (as disc) electrodes. In both cases it is demonstrated that, by applying suitable variable changes and the kss treatment, the boundary value problem (bvp) for the CEC mechanism can be reduced to a single diffusion-only differential equation with constant initial conditions and with a single surface condition that accounts for the influence of the chemical kinetics. The benefits in terms of simplicity, generality and calculation demands are discussed.

The problem corresponding to (hemi)spherical electrodes is solved analytically for single potential pulse techniques, being applicable to any electrode size scale where diffusion-based models are suitable (that is, to electrodes larger than 100 nm where the effects of the interfacial electric field can be neglected under excess of supporting electrolyte[15]). Illustrating the applicability of the treatment within the digital simulation of electrochemical experiments, the CEC response in cyclic voltammetry (CV) at (hemi)spherical and disc electrodes is simulated here and the equivalence relationship between the current-potential (I-E) response at disc and spherical electrodes is examined as affected by the incidence of homogeneous chemical kinetics.

The results presented here enable simple, accurate and rapid preliminary analysis of the intricate CEC mechanism, the establishment of the optimum conditions for their quantitative study, as well as the fast analysis of experimental data. The voltammetry of other reaction schemes derived from the CEC mechanism is discussed together with an experimental protocol for their elucidation and quantitative characterization through the analysis of the

electrochemical signal as a function of the experiment time-scale, the electrode size and the medium composition.

THEORY

Mathematical resolution of the CEC mechanism

Let us consider a Nernstian interfacial CT following a CEC mechanism with first-order chemical reactions as shown in Scheme (I) and equal diffusion coefficients for all the species (=*D*). Under these conditions, in SI-1 it is demonstrated for both uniformly (such as (hemi)spheres) and non-uniformly (such as discs) accessible electrodes that the modelling of the CEC mechanism can be reduced to the resolution of only one differential diffusion equation problem of variable $c_1 = c_B + c_C$ (Eqs. (23)-(25) of the Supporting Information). Depending on the electrode geometry and on the complexity of the voltammetric perturbation, such problem can be solved either analytically or numerically.

Analytical solution in spherical diffusion for single pulse techniques

In the case of uniformly-accessible electrodes, the exact solution can be obtained analytically for single pulse techniques. For the sake of example, it has been solved for spherical diffusion in SI-2, obtaining an explicit analytical solution for $c_1(r,t)$ (Eq. (S53)) and the following expression for the current-potential-time response, which is valid for any electrode radius from macro- to micro-electrodes:

$$\frac{I^{sp}}{I_{eq}^{sp}} = \delta_d^{sp} \frac{\Lambda^{sp}\left[1+K_2+\left(1+K_1\right)e^{\eta}\right]}{K_2+r_0\Lambda^{sp}\left[1+K_2+\left(1+K_1\right)e^{\eta}\right]}\left[1+\frac{2}{\sqrt{\pi}}r_0\Lambda^{sp}\left(\frac{1+K_2+\left(1+K_1\right)e^{\eta}}{K_2}\right)\frac{F(\chi^{sp})}{\chi^{sp}}\right] \quad (3)$$

where $\eta = \frac{F}{RT}(E-E^{0'})$ with E being the constant applied potential and $E^{0'}$ the formal potential of the redox couple C/D. In Eq. (3), I_{eq}^{sp} is the current corresponding to total electrochemical and chemical equilibrium conditions for a spherical electrode of surface area S:

$$I_{eq}^{sp} = FSD\frac{(c_1^* - c_{1,eq}^{sur})}{\delta_d^{sp}} \quad (4)$$

where $c_{1,eq}^{sur}$ is the surface value of c_1 under total equilibrium (electrochemical and chemical) conditions, which is independent of time and of the electrode geometry (section SI-1)[a]:

$$c_{1,eq}^{sur} = (c_1^* + c_2^*)\frac{(1+K_1)e^{\eta}}{1+K_2+(1+K_1)e^{\eta}} \tag{5}$$

with c_1^* and c_2^* being the total initial concentration of the oxidized ($c_1^* = c_B^* + c_C^*$) and reduced ($c_2^* = c_D^* + c_E^*$) species, respectively. δ_d^{sp} corresponds to the thickness of the linear diffusion layer for spherical electrodes[4]:

$$\delta_d^{sp} = \frac{1}{\left(\frac{1}{r_0} + \frac{1}{\sqrt{\pi D t}}\right)} \tag{6}$$

χ^{sp} in Eq. (3) is a dimensionless parameter that includes the influence of the homogeneous chemical kinetics and thermodynamics, and of the electrode sphericity:

$$\chi^{sp} = 2\sqrt{Dt}\left[\frac{1}{r_0} + \Lambda^{sp}\left(\frac{1+K_2+(1+K_1)e^{\eta}}{K_2}\right)\right] \tag{7}$$

with Λ^{sp} given by (see Table S1),

$$\Lambda^{sp} = \frac{K_2}{\delta_{r,1}^{sp}K_1(1+K_2) + \delta_{r,2}^{sp}K_2(1+K_1)e^{\eta}} \tag{8}$$

where $\delta_{r,i}^{sp}$ ($i = 1,2$) is the thickness of the linear reaction layers[4]:

$$\delta_{r,i}^{sp} = \frac{1}{\left(\frac{1}{r_0} + \sqrt{\frac{\kappa_i}{D}}\right)} \quad (i = 1,2) \tag{9}$$

with κ_i $(i = 1,2)$ as given by Eq. (2), and:

[a] Eq. (5) can also be deduced by taking into account that the Nernstian relationship holds at the electrode surface together with the assumption that chemical equilibrium relationships (Eq. (1)) holds for any values of the spatial coordinates (q) and time (t), and that the total concentration remains constant ($c_1(q,t) + c_2(q,t) = c_1^* + c_2^* = c_T^*$).

$$F(\chi^{sp}) = \sqrt{\pi}\,\frac{\chi^{sp}}{2} e^{(\chi^{sp}/2)^2}\,\mathrm{erfc}(\chi^{sp}/2) \tag{10}$$

that under equilibrium conditions ($\chi^{sp} \to \infty$), $F(\chi^{sp}) \to 1$ so that $I^{sp} = I^{sp}_{eq}$ in Eq. (3). Other particular cases of Eq. (3) can be found in Section SI-2.1: macroelectrodes (transient response), microelectrodes (with both transient and steady state responses, sensitive to the chemical kinetics) and ultramicroelectrodes (steady state response, insensitive to the chemical kinetics).

Numerical solution for spherical electrodes in multipulse techniques and for disc electrodes

The single-variable (c_1) problem given by Eqs. (23)-(25) of the Supporting Information can be solved very efficiently with 3-point approximations of the spatial derivatives via the simple tridiagonal Thomas algorithm[16–18], within the alternating direction implicit (ADI) method in the case of discs[16,17]. Thus, only the coefficients corresponding to the surface conditions being affected by the homogeneous chemical kinetics. At (hemi)spherical electrodes the dimensionless surface condition is given by:

$$T > 0, R = 1: \quad \left(\frac{\partial C}{\partial R}\right)_{R=1} = r_0 \Lambda^{sp} \left(\frac{1 + K_2 + (1 + K_1) e^{\eta(t)}}{K_2} \right) \left(C^{sur} - C^{sur}_{eq} \right) \tag{11}$$

and at discs by:

$$T > 0, 0 \le R \le R_0, Z = 0: \quad \left(\frac{\partial C}{\partial Z}\right)_{Z=0} = r_0 \Lambda^{disc} \left(\frac{1 + K_2 + (1 + K_1) e^{\eta(t)}}{K_2} \right) \left(C^{sur} - C^{sur}_{eq} \right) \tag{12}$$

where $C = c_1 / c_T^*$ (so that $C^{sur}_{eq} = c^{sur}_{1,eq} / c_T^*$), $R = r / r_0$, $Z = z / r_0$, $T = Dt / r_0^2$ [17], Λ^{sp} is given by Eq. (8) and:

$$\Lambda^{disc} = \frac{K_2}{\left\langle \delta^{disc}_{r,1} \right\rangle K_1 (1 + K_2) + \left\langle \delta^{disc}_{r,2} \right\rangle K_2 (1 + K_1) e^{\eta(t)}} \tag{13}$$

with[19,20]:

$$\left\langle \delta_{r,i}^{disc} \right\rangle = r_0 \frac{\pi}{4} \left\{ \frac{1 + 1.3650 r_0 \sqrt{\frac{\kappa_i}{D}} + 0.8826 r_0^2 \frac{\kappa_i}{D} + 0.32853 \left(r_0^2 \frac{\kappa_i}{D} \right)^{3/2} + 0.063566 \left(r_0^2 \frac{\kappa_i}{D} \right)^2}{1 + 2.0016 r_0 \sqrt{\frac{\kappa_i}{D}} + 1.8235 r_0^2 \frac{\kappa_i}{D} + 0.96367 \left(r_0^2 \frac{\kappa_i}{D} \right)^{3/2} + 0.307949 \left(r_0^2 \frac{\kappa_i}{D} \right)^2 + 0.049925 \left(r_0^2 \frac{\kappa_i}{D} \right)^{5/2}} \right\} \left(i = 1, 2 \right) \tag{14}$$

Then, the corresponding Thomas coefficients for a two-point approximation of the surface derivative are given by ($G \equiv sp, disc$):

$$\beta_0 = 1 + h r_0 \Lambda^G \left(\frac{1 + K_2 + \left(1 + K_1\right) e^{\eta(t)}}{K_2} \right) \quad , \quad \gamma_0 = -1 \quad , \quad \delta_0 = h r_0 \Lambda^G \left(\frac{1 + K_2 + \left(1 + K_1\right) e^{\eta(t)}}{K_2} \right) C_{eq}^{sur} \tag{15}$$

where h is the first spatial interval of the grid in the R-direction at (hemi)spheres and in the Z-direction at discs. It is worth noting that the treatment presented here enables us to perform the simulation with a single and optimized spatial grid, a simple and efficient resolution algorithm and reduced implementation and calculation times.

RESULTS AND DISCUSSION

The normal pulse voltammetry (NPV) curves in Figure 1 have been obtained for a spherical electrode of radius $r_0 = 50\ \mu m$ from the analytical equation (3). Figures 1A and 1B show the dimensionless current-potential responses ($I^{sp}/I^{sp}_{eq,lim}$ *vs* $(E - E^{0'})$) of the the CEC mechanism (black curves) as compared with the limit cases CE (Fig. 1A, blue curves) and EC (Fig. 1B, green curves). Regarding the position of the wave, the CE and EC responses are located at negative and positive potentials relative to a simple reversible CT (E_{rev} mechanism, in red), respectively. This reflects that the electron transfer (ET) is more difficult in a CE process than in an E_{rev} one, whereas the ET is facilitated by a subsequent chemical reaction. This behaviour is observed more clearly in Figures 1A' (CEC and CE mechanisms) and 1B' (CEC and EC mechanisms), where the shift of the half-wave potential ($E_{1/2} - E^{0'}$) is studied for the different mechanisms as a function of the chemical equilibrium (K_i, $i = 1,2$, Eq. (1)) and kinetic (κ_i, Eq. (2)) constants; the (red) plane at $E_{1/2} = E^{0'}$ corresponds to the E_{rev} mechanism. As can be seen, in the case of the CE and EC mechanisms, $\left|E_{1/2} - E^{0'}\right|$ increases with K_1 and κ_1 or with K_2 and κ_2, respectively. The position of the electrochemical signal of the CEC process shows a more complex behaviour that is intermediate between the CE and EC limits. Thus, the CEC signal appears at more positive potentials than an E_{rev} process when the extent of the subsequent reaction is larger than the preceding one and at more negative potentials in the contrary case. Obviously, the signal is situated at the same potential as an E_{rev} process (*i.e.*, $E_{1/2} = E^{0'}$) when the extent of both chemical reactions are equal. In the limit of very fast kinetics (total chemical equilibrium), the $E_{1/2}$-value of the CEC mechanism ($E^{eq}_{1/2}$) is given by (Eq. (4)):

$$E^{eq}_{1/2} = E^{0'} + \frac{RT}{F}\ln\left(\frac{1+K_2}{1+K_1}\right) \qquad (16)$$

that in the case $K_1 = K_2$ leads to $E^{eq}_{1/2} = E^{0'}$ (see Fig. 1A').

With respect to the magnitude of the NPV wave (that is, the limiting current, $I_{\text{lim}}^{\text{sp}}$), Figures 1A and 1B show that it is only determined by K_1 and κ_1 values so that the same $I_{\text{lim}}^{\text{sp}}$ value is obtained for CEC and CE processes (see black and blue curves in Fig. 1A). This behaviour is predicted by Eq. (3) that, when considering $E << E^{0'}$ ($e^{\eta} \to 0$), leads to an expression identical to that of the CE mechanism[10]:

$$\frac{I_{\text{lim}}^{\text{sp}}}{I_{\text{eq,lim}}^{\text{sp}}} = \delta_{\text{d}}^{\text{sp}} \frac{1}{K_1 \delta_{\text{r,1}}^{\text{sp}} + r_0} \left[1 + \frac{r_0}{\sqrt{\pi D t}} \left(\frac{r_0}{r_0 + K_1 \delta_{\text{r,1}}^{\text{sp}}} \right) F(\chi_{\text{lim}}^{\text{sp}}) \right] \tag{17}$$

where (Eq. (7)):

$$\chi_{\text{lim}}^{\text{sp}} = 2\sqrt{Dt} \left(\frac{1}{r_0} + \frac{1}{K_1 \delta_{\text{r,1}}^{\text{sp}}} \right) \tag{18}$$

and $I_{\text{eq,lim}}^{\text{sp}}$ is given by Eq. (4) with $c_{1,\text{eq}}^{\text{sur}} = 0$.

From Eq. (17) it is immediately inferred that the limiting current is only limited by the availability of the reactant species, determined by the geometry of the diffusion field and by the chemical conversion of B to C species (see Scheme (I)). Thus, as shown in Figures 1A and 1B, the limiting current increases when K_1 decreases and/or κ_1 increases. Eventually, in the limits $K_1 \to 0$ (EC mechanism) or $\kappa_1 >> 1$, the limiting current coincides with that of an E_{rev} mechanism (green curves in Fig. 1B and curves for K_1=5 and $\kappa_1 = 10^7$ s^{-1} in Fig. 1A), since the chemical kinetics in this last case is so fast that the interconversion between B and C is 'instantaneous'.

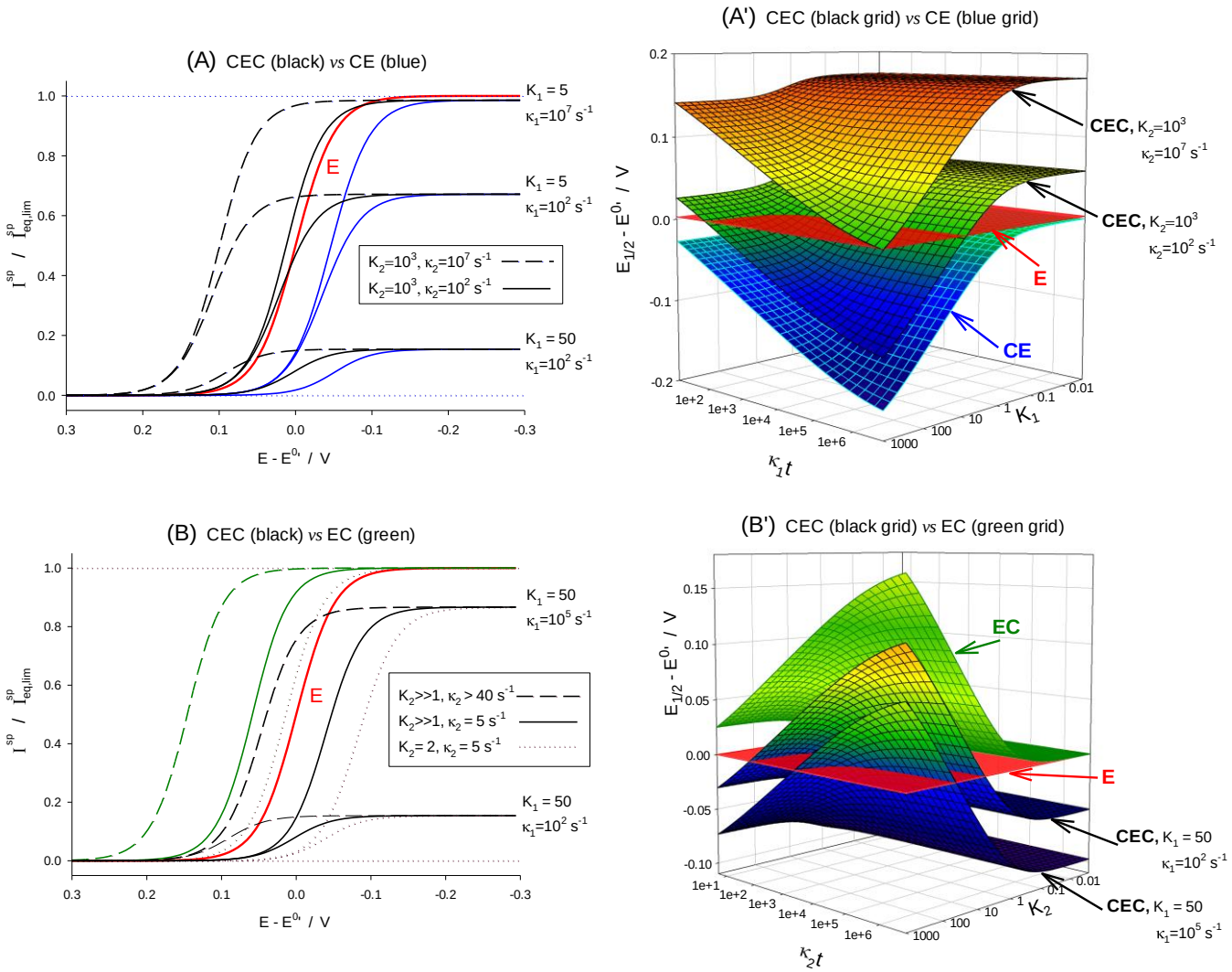

Figure 1. (A), (B): NPV response of the CEC (black lines), CE (blue lines) and EC (green lines) mechanisms at a spherical electrode with $r_0 = 50\ \mu m$ (Eq. (3)). **(A'), (B'):** Variation of the half-wave potential ($E_{1/2}$) of the CEC (black grids), CE (blue grid) and EC (green grid) mechanisms as a function of the kinetic and equilibrium constants of the reactions preceding (κ_1, K_1) **(A')** and following (κ_2, K_2) **(B')** the ET (Eq. (3)). In all cases, the E_{rev} mechanism is also plotted in red as a reference. $t = 1\ s$, $D = 10^{-5}\ cm^2/s$, T=298 K. $I^{sp}_{eq,lim} = FSDc_1^* / \delta^{sp}_d$.

Figure 2 shows the evolution of the CV response of a CEC process (solid lines) at a macroelectrode ($r_0 \to \infty$) for different values of the dimensionless kinetic constants, $\chi_{i,CV}$ ($= \kappa_i \frac{RT}{Fv}$ $(i = 1,2)$ where v is the scan rate) of the preceding and subsequent chemical reactions (considered as equal for the sake of simplicity). The responses of the CE (Fig. 2A, dashed lines) and EC (Fig. 2B, dashed lines) schemes are also plotted in order to conclude criteria and procedures for discrimination between the different mechanisms.

Regarding the forward scan, the differences in magnitude of the forward peak of the CEC and CE mechanisms (Fig. 2A) are scarce since the peak current is not significantly affected by the chemical reaction following the ET, being mainly determined by K_1 and κ_1. On the other hand, the position of the CEC and CE peaks differs more apparently as $\chi_{i,CV}$ increases, that is, as the rate constants increase and/or the scan rate decreases. In relation to the discrimination between the CEC and EC schemes (Fig. 2B), the magnitude of the forward CEC peak is smaller than in the EC peak, only becoming similar for very fast chemical kinetics (see black curves). Note the parallelism with the corresponding effects in NPV (Fig. 1).

With regard to the reverse scan, the reverse peak in the CE mechanism (Fig. 2A) is larger than in the CEC scheme since in the latter the signal is greatly affected by the subsequent chemical reaction. As expected, in Figure 2B, for both the CEC and EC mechanisms, the reverse peak is of comparable magnitude to the forward one for very small κ_2 values (red curves). Then, the occurrence of the subsequent chemical reaction leads to the disappearance of the reverse peak (green curves) due to the transformation of the electroactive species into an electroinactive form (species E, see Scheme (I)). Further increase of κ_2 leads to the gradual re-appearance of the reverse peak (blue curves). Eventually, it is again comparable to the forward peak in the limit of very fast kinetics where the interconversion between the electroactive and electroinactive forms is 'instantaneous'. Indeed, for $\kappa_1, \kappa_2 >> 1$, the voltammetric response of the CEC mechanism in any technique is totally equivalent to that of the CE and EC mechanisms just shifted according to the equilibrium constants (Eq. (16), see also Fig. 1).

At slow-medium chemical kinetics, the cyclic voltammograms of the CEC and CE mechanisms (see green curves in Fig. 2A and green solid curve in Fig. 2B) show a sigmoidal shape in the forward scan, which is striking for a macroelectrode. This result is due to that the chemical supply of species C balances that of mass transport under these *particular* kinetic conditions such that a time-independent flux is attained. In the reverse scan, the CEC mechanism again

shows no peak due to the inference of the subsequent chemical reaction, whereas the CE mechanism (green dashed curve in Fig. 2A) does show an apparent peak that points out the transient nature of the response[21].

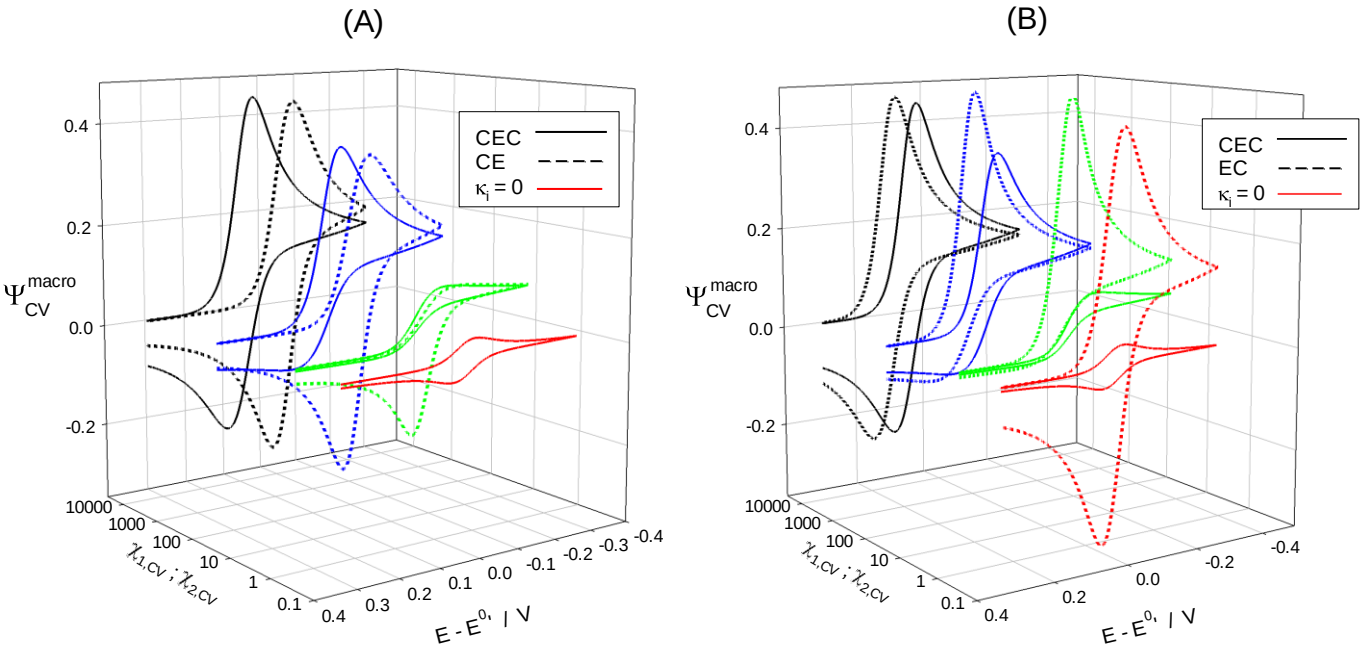

Figure 2. CV curves (Ψ_{CV}^{macro} vs $E-E^{0'}$) of the CEC mechanism (solid lines) as compared to **(A)** the CE and **(B)** EC mechanisms (dashed lines) at a macroelectrode for different values of the dimensionless chemical kinetics, $\chi_{i,CV}=\kappa_i\frac{RT}{Fv}$: 0 (red lines), 2.5 (green lines), $2.5\cdot10^2$ (blue lines) and $2.5\cdot10^4$ (black lines). K_1=10, K_2=100, v=100 mV/s, $D=10^{-5}$ cm^2/s, T=298 K. Curves have been obtained numerically as indicated in the Theory Section. $\Psi_{CV}^{macro}=\frac{I_{CV}^{macro}}{FSDc_1^*\sqrt{\frac{Fv}{DRT}}}$

The influence of the electrode geometry on the CV of the CEC_{irrev} ($K_2\rightarrow\infty$) mechanism is analysed in Figure 3 where the ratio between the maximum current density at discs and spheres ($\Psi_{CV,max}^{disc}/\Psi_{CV,max}^{sp}$) is studied as dependent on the chemical kinetics and/or the electrode size (see also Section SI-3). Unlike at macroelectrodes (where $\Psi_{CV,max}^{disc}=\Psi_{CV,max}^{sp}$), the $\Psi_{CV,max}^{disc}/\Psi_{CV,max}^{sp}$ value is larger than 1 and it shows a minimum at intermediate κ_i values both under transient ($r_0=20$ μm) and steady state ($r_0=1$ μm) conditions (see Section SI-2.1), being more apparent and situated at larger κ_i values as the electrode size decreases. This behaviour can be explained by the more efficient mass transport at microdiscs that leads to higher diffusive

flux but also to a smaller contribution of the preceding reaction to the current. Also note that this result evidences that the constant equivalence relationship between the I-E steady state response at disc and spherical microelectrodes of the same radius (ratio between the current densities = $4/\pi$[1,4]) breaks down when homogeneous chemical kinetic effects occur [22] (see curve for $r_0 = 1$ μm), even for Nernstian CTs.

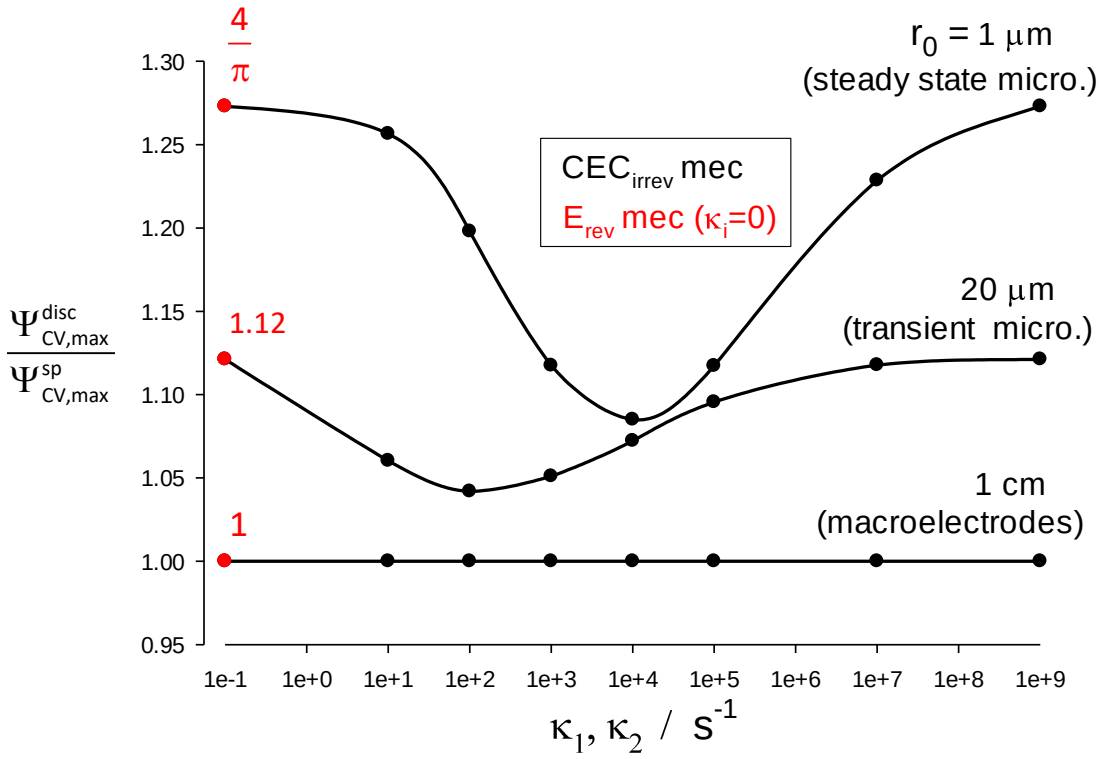

Figure 3. Ratio between the maximum CV current of the CEC_{irrev} ($K_2 \to \infty$) mechanism at disc and spherical electrodes as function of the chemical kinetics ($\kappa_1 = \kappa_2$ for the sake of simplicity) for different values of the electrode radius indicated on the figure. $\Psi^{G}_{CV,max}$ ($G \equiv sp, disc$) refers to the peak current for peak-shaped CV curves and to the plateau current for sigmoidal CV curves (see Figure S2 in SI-3). Other conditions and considerations as in Figure 2.

Experimental protocol

The identification and experimental characterization of the different possibilities within the general CEC scheme can be achieved through the following protocol, illustrated in the Experimental protocol graph:

Macroelectrodes

1. The comparison of the experimental limiting current chronoamperometry at macroelectrodes ($I_{\text{lim}}^{\text{macro,exp}}$) and the theoretical response $I_{\text{eq,lim}}^{\text{macro}}$ (Eq. (4) with $c_{1,\text{eq}}^{\text{sur}} = 0$ and $\delta_{\text{d}}^{\text{sp}}(r_0 \to \infty) \equiv \delta_{\text{d}}^{\text{macro}} = \sqrt{\pi Dt}$) reveals preceding chemical kinetic complications:

- **a.** If $I_{\text{lim}}^{\text{macro,exp}} = I_{\text{eq,lim}}^{\text{macro}}$, no chemical reaction occurs prior to the CT (E, EC or EC_{eq} mechanism) or it is (very) fast ($C_{eq}E$, $C_{eq}EC$ or $C_{eq}EC_{eq}$ mechanisms) (see Point 3 below).
- **b.** If $I_{\text{lim}}^{\text{macro,exp}} < I_{\text{eq,lim}}^{\text{macro}}$, there are chemical kinetic effects prior to the CT (CE, CEC or CEC_{eq} mechanisms), which can be characterized by fitting the experimental chronoamperograms with Eq. (17) for $r_0 \to \infty$, κ_1 and K_1 being the adjustable parameters.

2 and 2'. Subsequently, chemical complications following the CT can be elucidated from the values of the experimental NPV half-wave potential ($E_{1/2}^{\text{macro,exp}}$) and/or the magnitude of the experimental CV peak current in the backward scan ($I_{\text{CV,peak,back}}^{\text{macro,exp}}$):

- **a**. If $E_{1/2}^{\text{macro,exp}} = E_{1/2}^{\text{macro,1}}$ and/or $I_{\text{CV,peak,back}}^{\text{macro,exp}} = I_{\text{CV,peak,back}}^{\text{macro,1}}$ (where $E_{1/2}^{\text{macro,1}}$ and $I_{\text{peak,back}}^{\text{CV,1}}$ are the values deduced from Point 1 of the protocol with Eq. (3) and numerical simulation, respectively), the mechanism does not include any subsequent chemical reaction or this is (very) fast for being detected with a macroelectrode (CE, CEC_{eq}, E, $C_{eq}EC_{eq}$, $C_{eq}E$ or EC_{eq} mechanisms) (see Point 3 below).

b. If $E_{1/2}^{\text{macro,exp}} > E_{1/2}^{\text{macro,1}}$ and/or $\left|I_{\text{CV,peak,back}}^{\text{macro,exp}}\right| < \left|I_{\text{CV,peak,back}}^{\text{macro,1}}\right|$, the occurrence of a subsequent chemical kinetics can be concluded (CEC, EC or $C_{eq}EC$ mechanisms) and quantified (determining the κ_2 and K_2 values) by the analysis of the variation of $E_{1/2}^{\text{exp,macro}}$ with the pulse duration (t) from the theoretical I-E response given by Eq. (3) for $r_0 \to \infty$ and $e^{\eta} \to 0$, and/or of $I_{\text{CV,peak,back}}^{\text{macro,exp}}$ with the scan rate (v) via numerical simulations.

Microelectrodes

3. The study of (very) fast chemical kinetics requires the use of microelectrodes of suitable size (r_0) that warranties that the voltammetric signal is sensitive to the chemical kinetics, that is: $\frac{1}{K_i}\frac{\delta_d^G}{\delta_{r,i}^G} < 10$ (i=1,2) (see Section SI-2.1 and reference[10]). Then:

a. If $I_{\text{lim}}^{\text{micro,exp}} = I_{\text{eq,lim}}^{\text{micro}}$ (Eq. (17)) and $E_{1/2}^{\text{micro,exp}} = E_{1/2}^{\text{macro,exp}}$, the simple E_{rev} mechanism is confirmed.

b. If $I_{\text{lim}}^{\text{micro,exp}} = I_{\text{eq,lim}}^{\text{micro}}$ (Eq. (17)) and $E_{1/2}^{\text{micro,exp}} \neq E_{1/2}^{\text{macro,exp}}$, the EC mechanism holds and the corresponding kinetics (κ_2) can be characterized by comparison of the experimental data ($E_{1/2}^{\text{micro,exp}}$) with the theoretical predictions (*i.e.*, with the half-wave potential of the I-E response given by Eq. (3)) provided that K_2 is known from the previous Point 2'. Otherwise, studies with different pulse durations and/or electrode radii are necessary for the simultaneous determination of κ_2 and K_2.

c. If $I_{\text{lim}}^{\text{micro,exp}} < I_{\text{eq,lim}}^{\text{micro}}$, the existence of a preceding chemical reaction is inferred (CEC or CE mechanisms) and the corresponding κ_1 and K_1-values can be quantified from the experimental chronoamperogram ($I_{\text{lim}}^{\text{micro,exp}}$ vs t) with Eq. (17). Thus, the

theoretical half-wave potential can be calculated ($E_{1/2}^{micro,3c}$, from Eq. (3)) and compared with the experimental one ($E_{1/2}^{micro,exp}$) such that:

i. If $E_{1/2}^{micro,exp} = E_{1/2}^{micro,3c}$, a chemical reaction following the CT can be discarded: CE mechanism.

ii. If $E_{1/2}^{micro,exp} > E_{1/2}^{micro,3c}$, the inference of a subsequent chemical reaction can be concluded (CEC mechanism) and it can be characterized as discussed in the previous Point 3b.

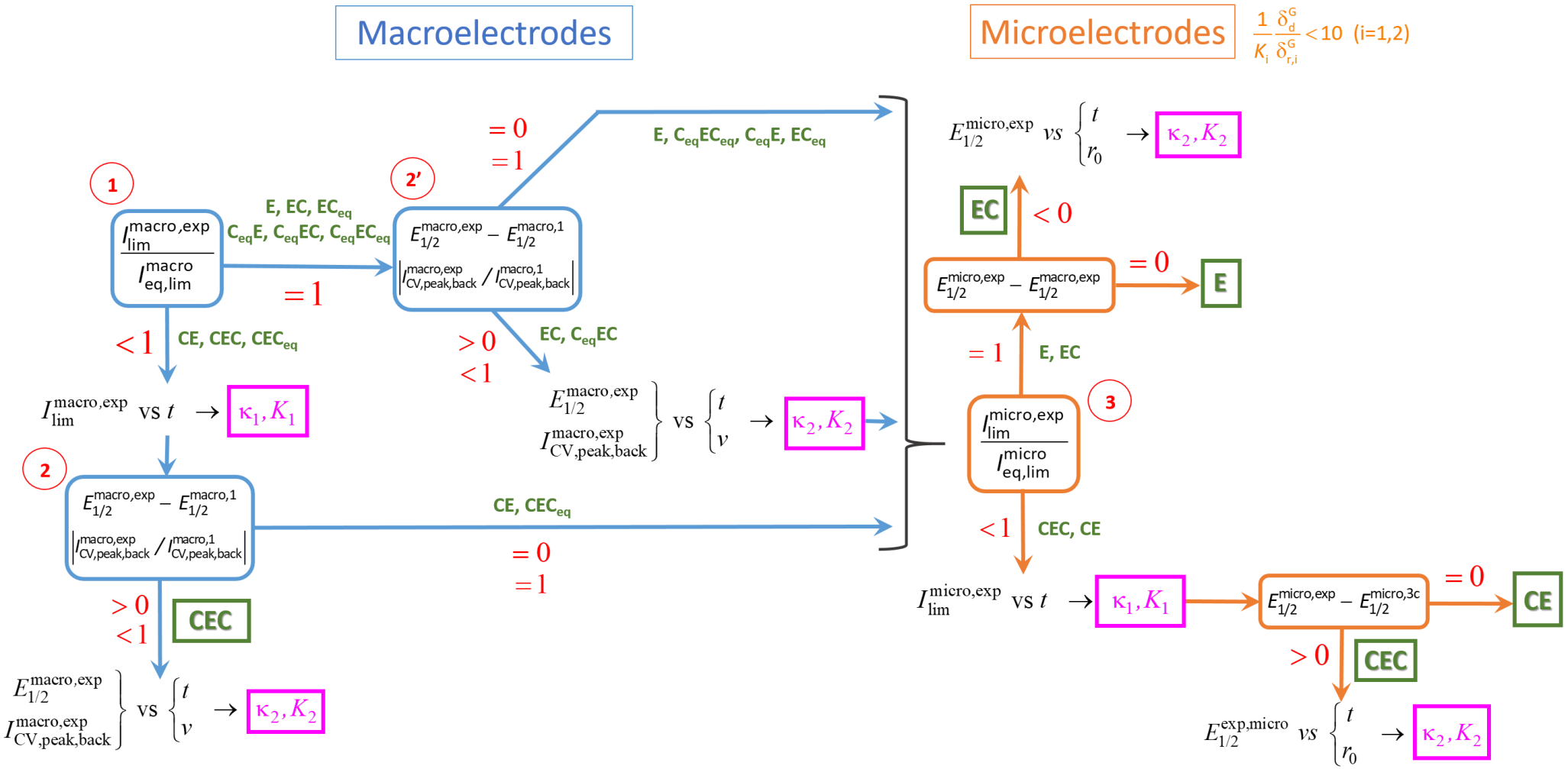

Experimental protocol graph. Guidelines for the elucidation and characterization of the different particular cases included in the CEC mechanism (see also Figure S3 for an extended protocol including the determination of the equilibrium constant of a C_{eq} step).

CONCLUSIONS

The suitable analysis of the boundary value problem leads to a remarkable generalization, simplification and acceleration of the theoretical treatment of homogeneous chemical reactions affecting the interfacial charge transfer whatever the electrode size and shape. Thus, the multivariable boundary value problem of the CEC mechanism at uniformly accessible (as (hemi)spheres) and non-uniformly accessible (as discs) electrodes has been reduced to a single variable problem. This is very beneficial for the mathematical resolution of the problem either by analytical or numerical methods.

The use of this treatment have been illustrated by obtaining analytical (single pulse techniques in spherical diffusion) and numerical (disc electrodes and cyclic voltammetry in spherical diffusion) solutions for the CEC mechanism for electrodes of any size. It is found that, when chemical kinetics coupled to the charge transfer occurs, the constant equivalence relationship between the steady state I-E response at microdiscs and micro(hemi)spheres (ratio between the current densities at electrodes of the same radius = $4/\pi$) does not hold in the presence of chemical kinetic effects even though the electron transfer is Nernstian.

The solutions presented enable a comprehensive study of the voltammetric response of the CEC mechanism as a function of the chemical rate and equilibrium constants and the electrode size and shape. As a result of the complete analysis carried out, clues and experimental protocols for the identification and characterization of coupled chemical reactions to the charge transfer and for the determination of kinetic and thermodynamic parameters from experimental data have been provided.

ACKNOWLEDGEMENTS

The authors greatly appreciate the financial support provided by the Fundación Séneca de la Región de Murcia (Project 19887/GERM/15).

ASSOCIATED CONTENT

Supporting Information

Boundary value problem of a single variable for the CEC mechanism at an arbitrary electrode geometry; Analytical solution of the CEC mechanism in single pulse techniques under spherical diffusion; Cyclic voltammetry of the CEC mechanism at (hemi)spherical and disc electrodes; Definitions of variables and parameters; Extended experimental protocol for the CEC mechanism.

REFERENCES

(1) Bard, A. J.; Faulkner, L. R. *Electrochemical Methods: Fundamentals and Applications*, 2nd ed.; Wiley: New York, 2001.

(2) Compton, R. G.; Banks, C. E. *Understanding Voltammetry*, 2nd ed.; Imperial College Press: London, 2010.

(3) Savéant, J. M. *Elements of Molecular and Biomolecular Electrochemistry: An Electrochemical Approach to Electron Transfer Chemistry*; John Wiley & Sons, 2006.

(4) Molina, A.; González, J. *Pulse Voltammetry in Physical Electrochemistry and Electroanalysis*; Scholz, F., Ed.; Monographs in Electrochemistry; Springer International Publishing: Berlin, 2016.

(5) Hammerich, O.; Speiser, B. *Organic Electrochemistry*; CRC Press: Boca Raton, 2016.

(6) Mellado, J. M. R.; Montoya, M. R. CEC Mechanisms in the Electroreduction of α-Dicarbonyl Compounds on Mercury Electrodes. *J. Electroanal. Chem.* **1994**, *365* (1–2), 71–78.

(7) Nekrassova, O.; Lawrence, N. S.; Compton, R. G. The Electrochemical Oxidation of 5-Thio-2-Nitrobenzoic Acid (TNBA) at a Boron Doped Diamond Electrode: Demonstration of a CEC Reaction. *Electroanalysis* **2003**, *15* (19), 1501–1505.

(8) Salehzadeh, H.; Nematollahi, D. Introducing CEC′ Mechanism: Electrochemical Oxidation of 4-Methylesculetin-Boric Acid Complex in the Presence of Glutathione. *Electrochim. Acta* **2013**, *111*, 909–915.

(9) Rafiee, M.; Nematollahi, D.; Salehzadeh, H. CEC Mechanism in Electrochemical Oxidation of Nitrocatechol–boric Acid Complexes. *Electrochim. Acta* **2011**, *56* (27), 9946–9952.

(10) Molina, A.; Morales, I.; López-Tenés, M. Chronoamperometric Behaviour of a CE Process with Fast Chemical Reactions at Spherical Electrodes and Microelectrodes. Comparison with a Catalytic Reaction. *Electrochem. commun.* **2006**, *8* (6), 1062–1070.

(11) Heyrovský, J.; Kůta, J. *Principles of Polarography*; Pub. House of Czechoslovak Academy of Sciences: Prague, 1965.

(12) Galus, Z. *Fundamentals of Electrochemical Analysis*; Ellis Horwood, 1994.

(13) Molina, A.; López-Tenés, M.; Laborda, E. Unified Theoretical Treatment of the Eirrev, CE, EC and CEC Mechanisms under Voltammetric Conditions. *Electrochem. commun.* **2018**, *92*, 48–55.

(14) Montenegro, M. I.; Queirós, M. A.; Daschbach, J. L. *Microelectrodes: Theory and Applications*; Springer Netherlands: Dordrecht, 1991.

(15) Smith, C. P.; White, H. S. Theory of the Voltammetric Response of Electrodes of Submicron Dimensions. Violation of Electroneutrality in the Presence of Excess Supporting Electrolyte. *Anal. Chem.* **1993**, *65* (23), 3343–3353.

(16) Britz, D.; Strutwolf, J. *Digital Simulation in Electrochemistry*; Monographs in Electrochemistry; Springer International Publishing: Cham, 2016.

(17) Compton, R. G.; Laborda, E.; Ward, K. R. *Understanding Voltammetry: Simulation of Electrode Processes*; Imperial College Press: London, 2014.

(18) Press, W. H.; Teukolsky, S. A.; Vetterling, W. T.; Flannery, B. P. *Numerical Recipes 3rd Edition: The Art of Scientific Computing*, 3 edition.; Cambridge University Press: Cambridge, UK ; New York, 2007.

(19) Molina, A.; Laborda, E.; González, J. The Reaction Layer at Microdiscs: A Cornerstone for the Analytical Theoretical Treatment of Homogeneous Chemical Kinetics at Non-Uniformly Accessible Microelectrodes. *Electrochem. commun.* **2016**, *71*, 18–22.

(20) Rajendran, L.; Sangaranarayanan, M. V. Diffusion at Ultramicro Disk Electrodes: Chronoamperometric Current for Steady-State EC' Reaction Using Scattering Analogue Techniques. *J. Phys. Chem. B* **1999**, *103*, 1518–1524.

(21) Savéant, J. M.; Vianello, E. Potential-Sweep Chronoamperometry Theory of Kinetic Currents in the Case of a First Order Chemical Reaction Preceding the Electron-Transfer Process. *Electrochim. Acta* **1963**, *8* (12), 905–923.

(22) Amatore, C.; Fosset, B. Equivalence between Microelectrodes of Different Shapes: Between Myth and Reality. *Anal. Chem.* **1996**, *68* (24), 4377–4388.

For Table of Contents Only